Seismic lateral pressures for design of rigid walls

Guoxi Wu and W.D. Liam Finn

Abstract: Design charts for seismic pressures against rigid walls subjected to horizontal earthquake shaking are presented for both uniform and nonuniform backfills. Solutions are based on a simplified model of soil response which gives results that agree almost exactly with rigorous solutions. Peak seismic thrusts are presented for three different soil profiles. For each profile, 250 combinations of ground accelerations and distributions of soil shear moduli with depth are analysed to provide data points of peak seismic thrust ratios for the construction of design envelopes. The seismic thrust ratios for design are presented as a function of the ratio of the predominant frequency of the earthquake motion and the fundamental frequency of the wall–soil system. An approximate method is given for evaluating the latter frequency without a full analysis.

Key words: rigid walls, seismic lateral pressures, design lateral pressures.

Résumé : L'on présente des abaques de calcul pour les pressions sismiques contre des murs rigides de remblais uniformes et non uniformes soumis à des secousses sismiques horizontales. Les solutions sont basées sur un modèle simplifié de réaction du sol qui donne des résultats qui concordent presque exactement avec les solutions rigoureuses. Les poussées de pic sont présentées pour trois différents profils de sol. Pour chaque profil, 250 combinaisons d'accélérations du terrain et de distributions des modules de cisaillement en fonction de la profondeur sont analysées pour fournir les données des points de pic des rapports de poussée sismique de pointe pour le tracé des enveloppes de calcul. Les rapports de poussée sismique sont présentés pour le calcul sous forme du rapport de la fréquence prédominante du tremblement de terre et de la fréquence fondamentale du système mur–sol. L'on donne une méthode approximative pour évaluer cette dernière fréquence sans devoir procéder à une analyse complète.

Mots clés : murs rigides, pressions sismiques latérales, calcul des pressions latérales.

[Traduit par la Rédaction]

Introduction

The Mononobe–Okabe method (Mononobe and Matsuo 1929; Okabe 1926) is commonly used to determine the magnitude and distribution of seismic pressure on a retaining wall. It is a modification of Coulomb's classic earth pressure theory which takes into account the inertia forces on a potential sliding wedge caused by earthquake accelerations. A detailed evaluation of the Mononobe–Okabe method has been reported by Seed and Whitman (1970). One of the basic requirements of the Mononobe–Okabe method is that the wall should move sufficiently to create a limit-equilibrium state in the backfill. This condition is not satisfied by rigid walls.

Several researchers have used elastic wave theory to derive seismic soil pressure against a rigid wall. Matsuo and Ohara (1960) obtained an approximate elastic solution using a two-dimensional analytical model. They simplified the problem by assuming zero vertical displacement ($v = 0$) in the soil mass. This simplification leads to infinitely large wall pressure when Poisson's ratio of the soil, μ, is equal to 0.5, as in a fully saturated undrained backfill. Scott (1973) used a one-dimensional elastic shear beam connected to the wall by Winkler springs to model the seismic effects of the backfill. A study by Veletsos and Younan (1994) concluded that Scott's model does not adequately describe the response of the system and may lead to large errors.

Wood (1973) provided analytical solutions for the response of a rigid wall retaining elastic uniform soil backfill of finite length subjected to harmonic base excitation. However, Wood's solution is mathematically complicated to apply in engineering practice and is limited to harmonic input motions.

Wood (1973) suggested an approximate static solution that gave very good estimates of the peak seismic thrust for harmonic excitation when dynamic amplification effects in the wall–soil system were negligible. He found dynamic amplification to be negligible when the frequency ratio $\Omega = f/f_s$ is less than about 0.5, where f is the frequency of harmonic motion, and $f_s = V_s/4H$ is the cyclic frequency of the first shear mode of the backfill considered as a semi-infinite layer of depth H, with shear wave velocity, V_s.

In the cases of a wide backfill and a peak horizontal acceleration A_{max}, the lateral seismic force F_{sr} against the wall when $\Omega < 0.5$ is given approximately for $\mu = 0.4$ by

$$[1] \qquad F_{sr} = \gamma H^2 k_h = \rho H^2 A_{max}$$

Received January 13, 1998. Accepted January 22, 1999.

G. Wu. Klohn–Crippen Consultants Ltd., 10200 Shellbridge Way, Richmond, BC V6X 2W7, Canada.
W.D.L. Finn.[1] Department of Civil Engineering, The University of British Columbia, 2324 Main Mall, Vancouver, BC V6T 1Z4, Canada.

[1]Author to whom all correspondence should be addressed.

Table 1. Analyses conducted for determining seismic thrusts.

Key soil parameters			No. of analyses		
L/*H*	μ	λ (%)	Uniform *G* (closed-form solution)	Parabolic *G* (finite-element solution)	Linear *G* (finite-element solution)
5.0	0.4	10	250	250	250
3.0	0.4	10	250	250	250
1.5	0.4	10	250	250	250
5.0	0.4	20		250	
5.0	0.4	5		250	
5.0	0.5	10		250	
5.0	0.3	10		250	

acting at a height of about 0.63*H* above the back of the wall, where γ is the unit weight, and k_h is the horizontal seismic coefficient. This solution by Wood (1973) is often used in practice because of its simplicity.

Arias et al. (1981) modelled the elastic backfill using a modification of the conventional shear beam model which included horizontal normal stresses and developed analytical expressions for the response of the wall to both harmonic and seismic excitation. Veletsos and Younan (1994) presented analytical solutions for the response of a semi-infinite, uniform viscoelastic soil medium. Their model with the assumption of no vertical stresses ($\sigma_y = 0$) works well for a wall with a semi-infinite backfill, but the results are less satisfactory for a finite backfill. Veletsos et al. (1995) adopted the Arias et al. model in their analyses of rigid walls with backfills of finite length rather than the model with a more exact expression for shear stress used by Veletsos and Younan.

A modified shear beam model that includes all previous models as special cases was developed and validated by Wu (1994), Finn et al. (1994), and Wu and Finn (1996). The modified shear beam model is applicable to both finite and semi-infinite backfills. Analytical solutions have been developed for uniform elastic backfills and finite-element solutions for nonhomogeneous elastic and nonlinear backfills. The elastic analytical solutions have been validated by comparison with the exact solutions of Wood (1973). Comparisons with the other approximate elastic solutions showed that the modified shear beam model gives results closer to the Wood solution over all ranges of significant variables (Wu 1994; Finn et al. 1994; Wu and Finn 1996).

The ultimate objective of this paper is to present design charts for seismic thrusts against rigid walls under earthquake excitations for uniform and nonuniform soil backfills. A closed-form solution of the modified shear beam model has been used to compute the thrusts for uniform soil profiles. A finite-element program incorporating the modified shear beam model has been used to compute the dynamic thrusts for nonuniform soil profiles. To cover many variations of soil stiffness and seismic motion from site to site and earthquake to earthquake, 250 combinations of 10 different accelerograms and 25 different distributions of shear moduli are analysed for each soil profile. The various analyses are described in Table 1. Peak seismic thrust ratios are presented as functions of the ratio of the predominant frequency of the earthquake motions to the fundamental frequency of the wall–soil system. An approximate procedure for estimating the latter frequency is given in the Appendix.

Fig. 1. (*a*) Geometry and boundary conditions for rigid walls. (*b*) Equivalent reduced wall–soil problem based on antisymmetric horizontal stress conditions.

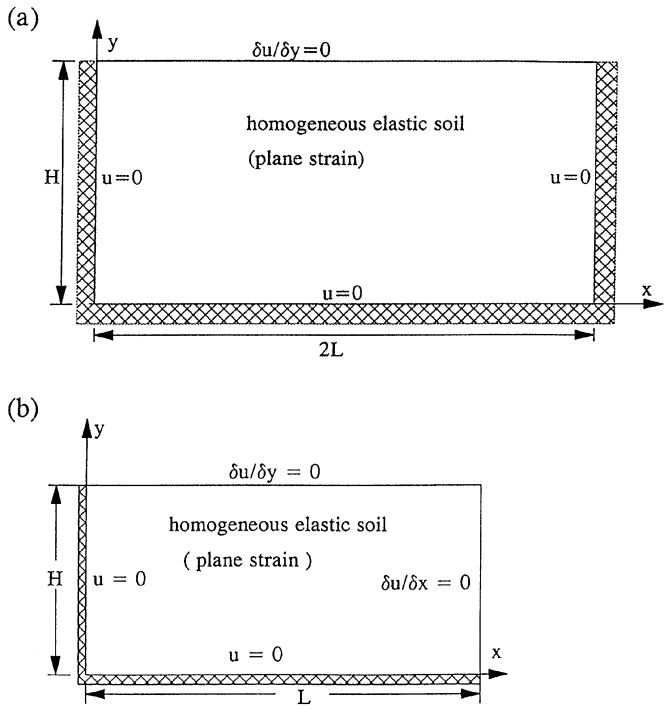

Thrust ratios at the upper bound and 84th percentile level are presented for use in the design of rigid walls under earthquake loading.

Analytical solutions for homogeneous soil backfills

The theory of the modified shear beam model and the different types of solutions can be found in Wu (1994) and Wu and Finn (1996). Only the basic equations needed to understand the process for estimating the seismic pressures are presented herein.

Analytical approximation of the problem

Figure 1*a* shows the geometry of the problem and the associated boundary conditions. A uniform elastic soil medium is confined by two vertical rigid walls and a rigid base. The soil layer has a total length of 2*L* and a height of *H*. When subjected to horizontal seismic motions, the soil medium in the system generates an antisymmetric field of horizontal normal stresses σ_x with $\sigma_x = 0$ at $x = L$. Therefore the original wall–soil problem can be represented more simply as shown in Fig. 1*b*. It is shown later that seismic pressures do not change for $L/H \geq 5.0$. Therefore, $L/H = 5.0$ is taken as the boundary between finite and semi-infinite backfills. The input seismic motions are applied at the rigid base. Since the rigid walls are rigidly connected to the base, the motions of rigid walls are identical to the input seismic motion.

Initially, the soil is assumed to be a homogeneous, isotropic, viscoelastic solid with a mass density ρ, a shear modulus *G*, and Poisson's ratio μ. Damping of the soil is modelled by applying constant damping to all modes of the wall–soil system.

Only the predominant horizontal displacement, *u*, has been taken into account in the analysis in order to simplify the solution of the problem. It will be shown later that this simplification does not introduce significant error in the solution and that very reliable estimates of the seismic thrust can be obtained using the proposed simplified model. Displacement used in the solution is the relative displacement between the backfill and the rigid base during shaking.

The equation of motion of the backfill for forced vibration due to base acceleration $\ddot{u}_b(t)$ is given by

$$[2] \qquad G\frac{\partial^2 u}{\partial y^2} + \frac{2}{1-u}G\frac{\partial^2 u}{\partial x^2} - \rho\frac{\partial^2 u}{\partial t^2} = \rho\ddot{u}_b(t)$$

and the normal stress in the *x* direction σ_x by

$$[3] \qquad \sigma_x = \frac{2}{1-\mu}G\frac{\partial u}{\partial x}$$

Using appropriate boundary conditions, the angular natural frequencies of the wall–soil system are found to be

$$[4] \qquad \omega_{mn} = \sqrt{\frac{G}{\rho}\left(b_n^2 + \frac{2}{1-\mu}a_m^2\right)}$$

where

$$[5] \qquad a_m = \frac{(2m-1)\pi}{2L} \qquad m = 1, 2, 3, \ldots$$

$$[6] \qquad b_n = \frac{(2n-1)\pi}{2H} \qquad n = 1, 2, 3, \ldots$$

The fundamental frequency ω_{11} corresponding to $m = 1$ and $n = 1$ is

$$[7] \qquad \omega_{11} = \frac{\pi}{2H}\sqrt{\frac{G}{\rho}}\sqrt{1 + \frac{2}{1-\mu}\frac{H^2}{L^2}}$$

Using the method of separation of variables, the transient displacement $u(x,y,t)$ in eq. [2] is found to be

$$[8] \qquad u(x,y,t) = \sum_{m=1}^{\infty}\sum_{n=1}^{\infty} \sin(a_m x)\sin(b_n y)\,\alpha_{mn}\,f_{mn}(t)$$

Where $f_{mn}(t)$ is a transient modal solution corresponding to the modal angular frequency ω_{mn}, and α_{mn} is the mode-participation factor given by

$$[9] \qquad \alpha_{mn} = \frac{16}{(2m-1)(2n-1)\pi^2}$$

Viscous damping of the wall–soil system is incorporated by using a modal damping ratio λ for each mode. In the case of damped forced vibration, the transient modal solution $f_{mn}(t)$ is obtained from the following equation:

$$[10] \qquad \ddot{f}_{mn}(t) + 2\lambda\omega_{mn}\dot{f}_{mn}(t) + \omega_{mn}^2 f_{mn}(t) = -\ddot{u}_b(t)$$

where $f_{mn}(t)$, $\dot{f}_{mn}(t)$, and $\ddot{f}_{mn}(t)$ are the relative displacement, velocity, and acceleration of a single degree of freedom system with an angular frequency ω_{mn} and damping ratio λ subjected to a base acceleration $\ddot{u}_b(t)$.

Dynamic wall pressures

The dynamic pressure distribution along the wall is

$$[11] \qquad p(t) = \frac{2G}{1-\mu}\sum_{m=1}^{\infty}\sum_{n=1}^{\infty} a_m\alpha_{mn}\sin(b_n y)\,f_{mn}(t)$$

The total dynamic thrust ($Q(t)$) acting on the wall is then given by integration of soil pressure over the height of the wall:

$$[12] \qquad Q(t) = \int_0^H p(t)\,dy = \frac{2G}{1-\mu}\sum_{m=1}^{\infty}\sum_{n=1}^{\infty}\frac{a_m\alpha_{mn}}{b_n}f_{mn}(t)$$

or

$$[13] \qquad Q(t) = \frac{2G}{1-\mu}\sum_{m=1}^{\infty}\sum_{n=1}^{\infty}\frac{16\,f_{mn}(t)}{\pi^2(2n-1)^2 L/H}$$

For a harmonic base acceleration $\ddot{u}_b(t) = A_{max}e^{i\omega t}$, the steady-state response $f_{mn}(t)$ is found from eq. [10] to be

$$[14] \qquad f_{mn}(t) = -\frac{A_{max}}{(\omega_{mn}^2 - \omega^2) + 2i\lambda\omega_{mn}\omega}e^{i\omega t}$$

Static solution and model verification

A simple verification of the model is provided by examining the static solution corresponding to the case when the period of the harmonic base excitation becomes infinitely long. The static solution is obtained by applying a uniform horizontal acceleration $\ddot{u}_b(t) = A_{max}$. The static thrust per unit length of the wall is

$$[15] \qquad Q^{st} = \frac{2G}{1-\mu}\frac{16A_{max}}{\pi^2 L/H}\sum_{m=1}^{\infty}\sum_{n=1}^{\infty}\frac{1}{(2n-1)^2\omega_{mn}^2}$$

Static solutions for walls with $L/H = 5.0$ and $L/H = 1.5$ using the models described above were compared with the exact solutions of Wood (1973) by Wu (1994), Finn et al. (1994), and Wu and Finn (1996). These evaluation studies

Fig. 2. Comparison of the accuracy of approximate solutions for rigid-wall systems for (*a*) $L / H = 5.0$ and (*b*) $L / H = 1.5$.

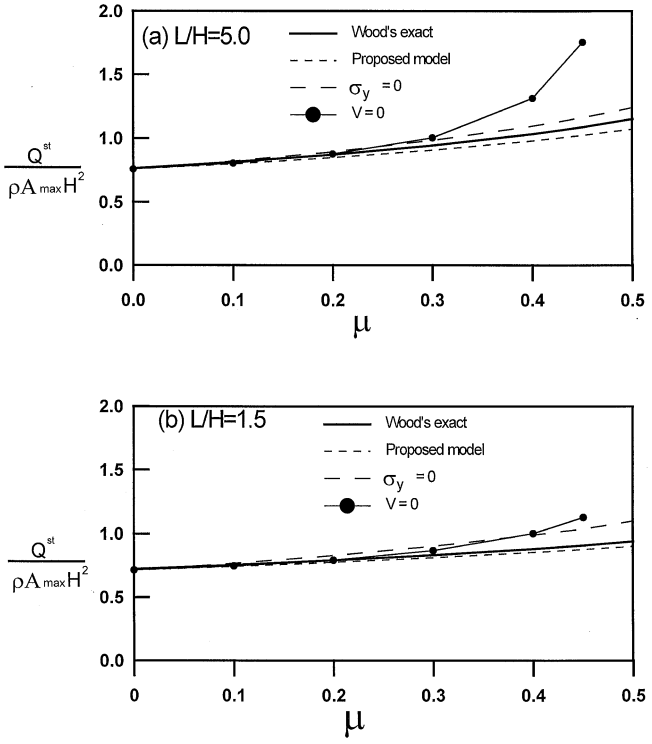

Fig. 3. The six-node finite element used in the analysis.

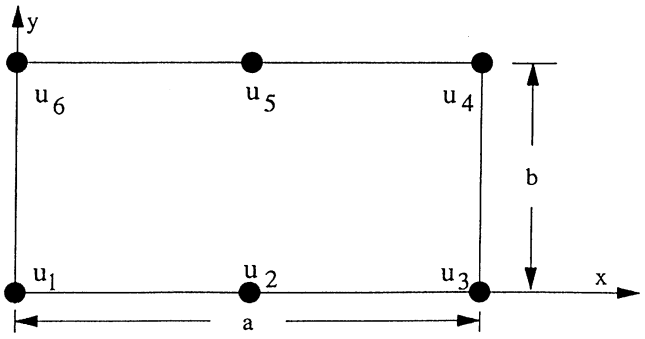

Fig. 4. Finite-element mesh used in the analysis.

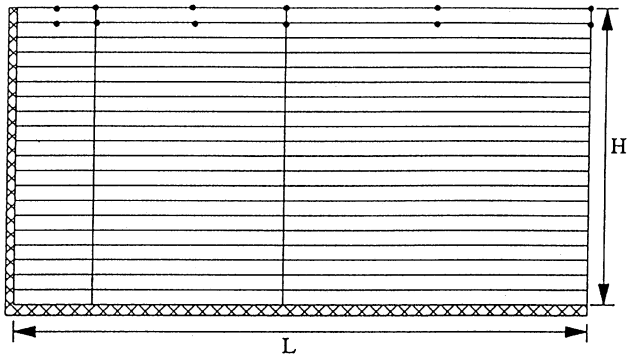

Fig. 5. Comparison of dynamic thrusts from finite-element (FE) and closed-form solutions for uniform backfill with $L / H = 1.5$.

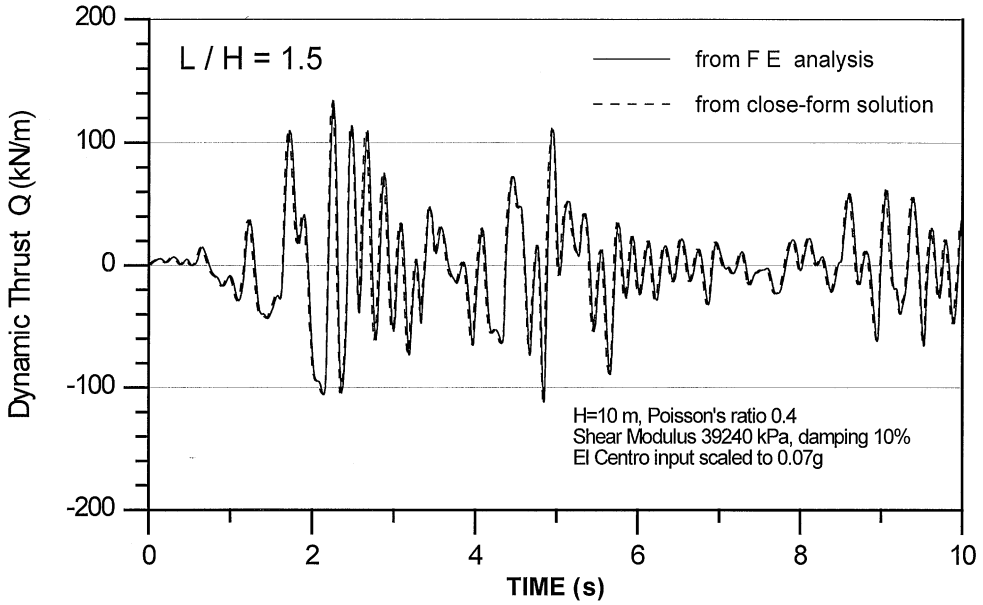

show that the modified shear beam model gives the best approximation to solutions for rigid wall systems with both infinite and finite backfills (Fig. 2).

Finite-element solutions for nonhomogeneous soil backfills

Nonhomogeneous soil backfills are modelled using the finite-element method. A six-node finite element (Fig. 3) which has six horizontal degrees of freedom is used to model the response of a soil element. The element has a quadratic variation of displacement u in the horizontal x direction and a linear variation in the vertical y direction. The finite-element mesh used in all analyses is shown in Fig. 4.

The finite-element response is compared with the results from the closed-form solution for a homogenous soil backfill in Fig. 5. The results of the two analyses are almost identical, confirming the accuracy of the finite-element representation.

Pressures for design

The dynamic pressures are computed for three types of soil profile, namely uniform, linear, and parabolic variations in shear modulus, G, with depth. For the latter two cases, the shear moduli G are assumed to vary from zero at the ground surface to G_{soil} at the bottom of the soil profile as shown in Fig. 6. A Poisson's ratio of $\mu = 0.4$ and a damping ratio of $\lambda = 10\%$ were used to establish the basic design curves. Additional analyses were conducted to study the effects of μ and λ on seismic pressures. The results of these analyses are presented later.

The seismic pressures are presented as a function of the fundamental frequencies of the wall–soil systems. These frequencies are computed directly during the analysis. However, to facilitate the use of design charts in practice, an approximate procedure for determining the fundamental frequencies is given in the Appendix.

Harmonic base excitation $\ddot{u}_b(t) = A_{max}e^{iwt}$

The peak dynamic thrusts at steady state for various combinations of L/H and soil profile were obtained using the modified shear beam model and are presented in Fig. 7. The normalized thrust ratios ($Q/\rho H^2 A_{max}$) are shown as functions of frequency ratios (ω/ω_{11}), in which ω represents the angular frequency of the excitation and ω_{11} represents the fundamental angular frequency of the wall–soil system.

For backfills of uniform G, the static thrusts corresponding to infinitely low excitation frequency ω are $1.0\,\rho H^2 A_{max}$ for $L/H = 5.0$ and $0.86\,\rho H^2 A_{max}$ for $L/H = 1.5$. The dynamic thrusts increase as the excitation frequency approaches the fundamental frequency of the wall–soil system. At resonant conditions, the peak dynamic thrusts are $2.4\,\rho H^2 A_{max}$ for $L/H = 5.0$ and $3.0\,\rho H^2 A_{max}$ for $L/H = 1.5$, giving dynamic amplification factors of 2.4 for $L/H = 5.0$ and 3.5 for $L/H = 1.5$, respectively. The results suggest that the dynamic amplification for wall–soil systems with finite backfills is larger than that for wall–soil systems with semi-infinite backfills for harmonic excitation.

For nonhomogeneous backfills with $L/H = 5.0$, the static thrusts are about $0.82\,\rho H^2 A_{max}$ for backfills of parabolic G and $0.71\,\rho H^2 A_{max}$ for backfills of linear G. At resonance the peak corresponding dynamic thrusts are $1.87\rho H^2 A_{max}$ and $1.56\,\rho H^2 A_{max}$, giving dynamic amplification factors of 2.3 and 2.2, respectively.

For all cases under harmonic base excitation, the peak dynamic thrusts at steady state are quite consistent with the magnitude of the static thrust up to a frequency ratio $\omega/\omega_{11} = 0.5$. This means that the static solution of Wood (1973) can be applied for estimating the peak dynamic thrusts under harmonic excitation for $\omega/\omega_{11} \le 0.5$ as shown in Fig. 7. However, as shown in later sections, the static solution of Wood may significantly underestimate the magnitude of dynamic thrusts under seismic loading for a frequency ratio $\omega/\omega_{11} > 0.2$.

Seismic base excitation

Seismic base motions are represented by the 10 accelerations recorded during the earthquake events identified in Table 2. The time histories of the input accelerations are shown in Fig. 8. These earthquake accelerations are selected to cover a range of shaking intensities and excitation frequencies. The predominant frequencies of each accelerogram cor-

Fig. 6. Three representative types of soil profiles.

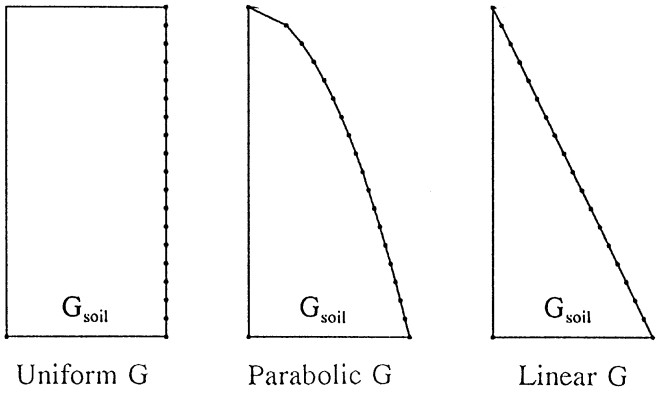

Fig. 7. Peak dynamic thrusts for steady-state harmonic excitation.

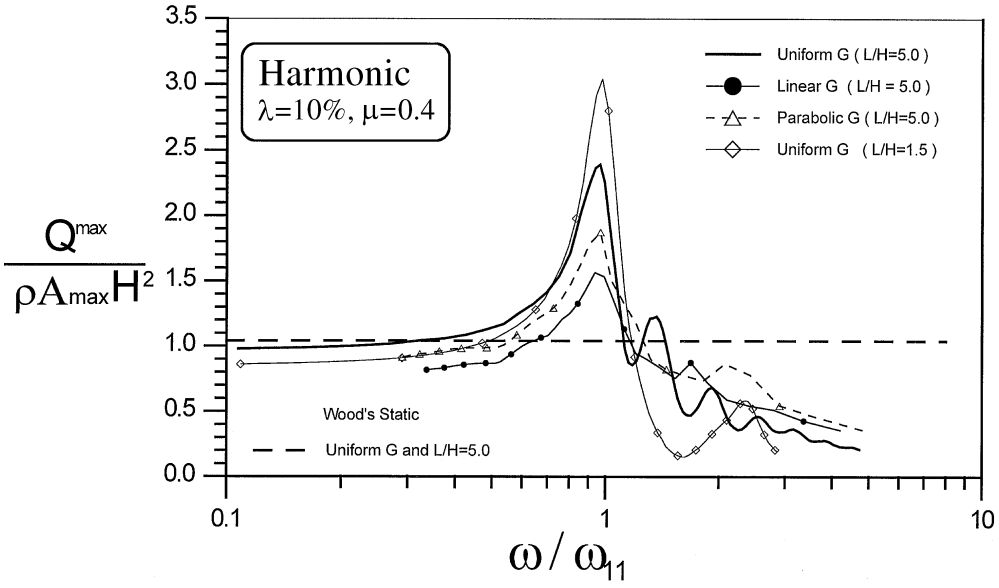

Fig. 8. Time histories of 10 seismic accelerograms used in the analyses.

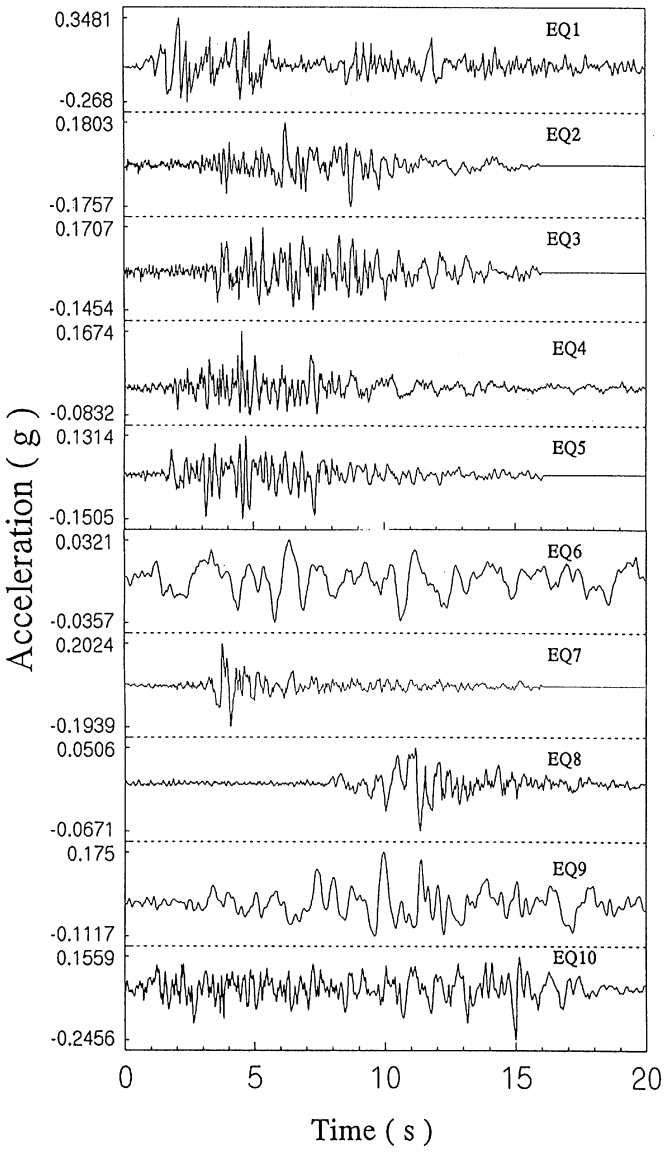

responding to peak spectral acceleration are given in Table 2.

The peak seismic thrusts are computed for each soil profile (Fig. 6) under earthquake loads represented by the 10 accelerograms. For each soil profile, analyses were conducted with 25 different values of G_{soil} to simulate the range of soil stiffnesses at different sites and the changes in shear moduli due to softening caused by dynamic shear strains.

Two hundred and fifty data points of peak seismic thrust ratios, $Q^{max}/\rho A_{max}H^2$, for backfills with L/H = 5.0 are shown in Figs. 9–11 for soil profiles of uniform G, parabolic G, and linear G, respectively. A upper bound curve and an 84th percentile curve for seismic thrust ratios are given in each figure. The static solution of Wood (1973) for a uniform backfill is shown in each figure because it is used in practice to estimate seismic thrust whether the backfill is uniform or not.

Analyses were also conducted to determine the seismic thrust ratios, $Q^{max}/\rho A_{max}H^2$, against rigid walls retaining backfills of finite length, represented by L/H = 3.0 and 1.5. The peak seismic thrust ratios for the L/H = 1.5 case are shown in Figs. 12–14 for the soil profile of uniform G, parabolic G, and linear G, respectively. The data points for the L/H = 3.0 case are not shown here because of space limitation.

The 84th percentile curves of peak seismic thrust ratios, $Q^{max}/\rho A_{max}H^2$, which are considered a suitable level for design are shown in Figs. 15–17 for backfills with L/H = 5.0, 3.0, and 1.5, respectively. For each L/H ratio, the 84th percentile curves for uniform G, parabolic G, and linear G are presented. The static solutions of Wood (1973) corresponding to the case of uniform G are also shown in Figs. 15–17. The heights of application of the seismic thrusts are shown in Fig. 18. The heights of application are fairly constant over the entire range of ω/ω_{11} ratio for each soil profile.

The following observations are made with respect to results presented in Figs. 9–18:

•The soil backfill with uniform G results in the largest seismic pressures, and the soil backfill with linear G results in the smallest seismic pressures.

•Dynamic amplification of seismic thrusts increases as the L/H ratio decreases from 5.0 to 1.5. The peak dynamic

Table 2. Characteristics of seismic accelerograms used in the analyses.

	Description					
Accelerogram	Year	Earthquake	Station	Component	Peak spectral acceleration (g)	Angular frequency of the excitation (rad/s)
EQ1	1940	El Centro	Imperial Valley, Calif.	S00E	0.348	11.64
EQ2	1971	San Fernando	Griffith Park, Los Angeles	S00E	0.180	25.13
EQ3	1971	San Fernando	Griffith Park, Los Angeles	S90E	0.171	25.13
EQ4	1971	San Fernando	Lankershim St., San Fernando	S00E	0.167	31.4
EQ5	1971	San Fernando	Lankershim St., San Fernando	S90E	0.151	25.13
EQ6	1985	Mexico City[a]	—	—	0.0357	7.0
EQ7	1979	Monte Negro	Bar, City Hall	S00E	0.202	12.57
EQ8	1989	Loma Prieta	Yerba Buena Island, Calif.	S90E	0.0671	10.13
EQ9	1989	Loma Prieta	Stanford University, Stanford, Calif.	S00E	0.175	10.47
EQ10	1949	Puget Sound[b]	—	—	0.246	18.0

[a]Partial segment of a rock motion recorded during the 1985 Mexico City earthquake.

[b]Artificial accelerogram; modified from a recorded accelerogram of the Puget Sound earthquake.

Fig. 9. Peak seismic thrusts for soil profiles with uniform *G*.

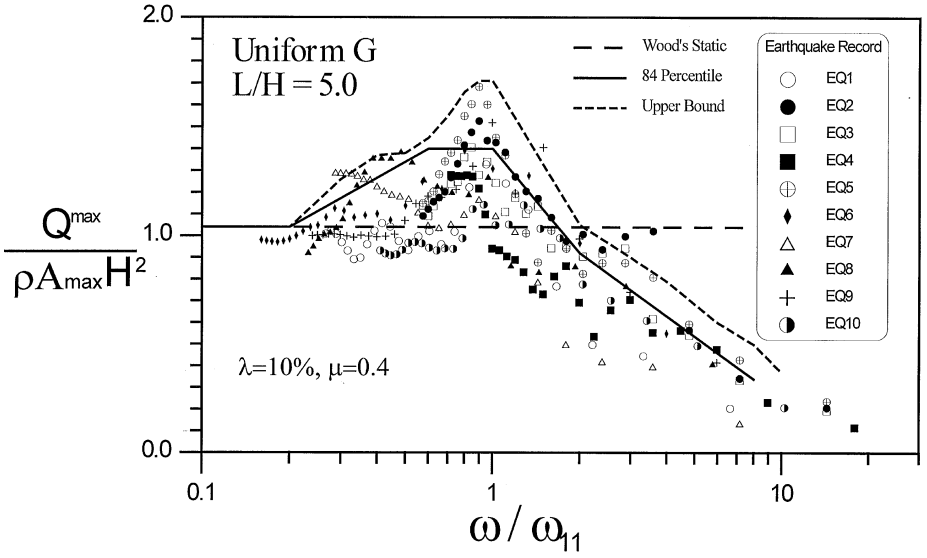

Fig. 10. Peak seismic thrusts for soil profiles with parabolic variation in *G*.

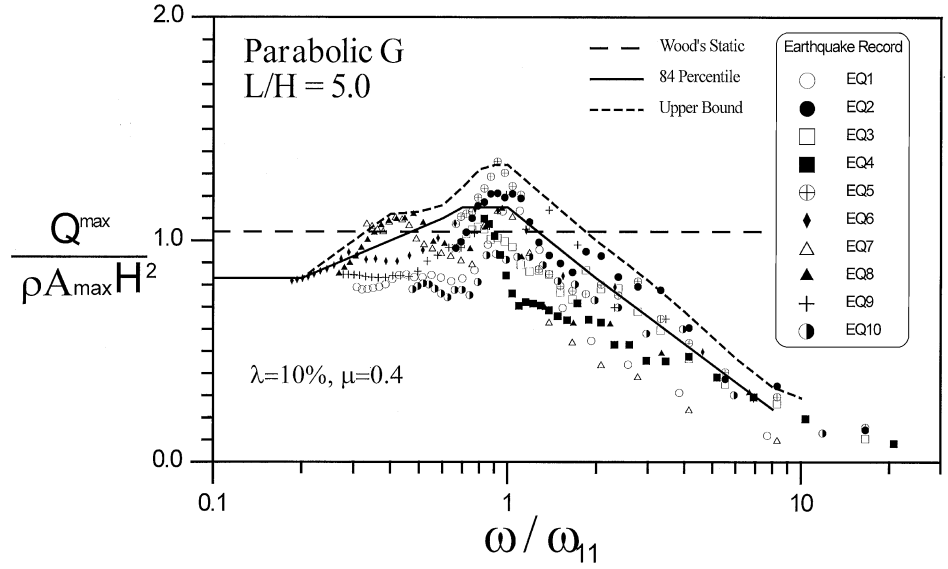

thrusts close to resonance (ω/ω_{11} = 0.7 to 1.0) are greater for backfills with L/H = 1.5 than for backfills with L/H = 5.0, although the dynamic thrusts at a very low frequency ratio ($\omega/\omega_{11} \leq 0.1$) are lower for backfills with L/H = 1.5 than for backfills with L/H = 5.0.

•Seismic excitation results in significant dynamic amplification for a wider range of frequency ratios than does harmonic excitation.

•For the soil profile with uniform *G* considered by Wood (1973), static thrusts from his analyses of harmonic motions are significantly lower than the peak dynamic thrusts due to earthquake excitation for frequency ratios between 0.2 and 2.0 but higher than the peak dynamic thrusts for frequency ratios greater than 2.0.

•The 84th percentile of the peak seismic thrusts against walls with semi-infinite backfills (L/H = 5) could reach 1.4 $\rho H^2 A_{max}$ for a uniform modulus profile, 1.15 $\rho H^2 A_{max}$ for a parabolic modulus profile, and 1.0 $\rho H^2 A_{max}$ for a linear modulus profile.

•For backfills with L/H = 3.0, the 84th percentile of the peak seismic thrusts could reach 1.55 $\rho H^2 A_{max}$ for a uniform modulus profile, 1.25 $\rho H^2 A_{max}$ for a parabolic modulus profile, and 1.1 $\rho H^2 A_{max}$ for a linear modulus profile.

•For backfills with L/H = 1.5, the 84th percentile of the peak seismic thrusts could reach 1.6 $\rho H^2 A_{max}$ for a uniform modulus profile, 1.3 $\rho H^2 A_{max}$ for a parabolic modulus profile, and 1.2 $\rho H^2 A_{max}$ for a linear modulus profile.

•The peak seismic thrust decreases significantly for frequency ratios $\omega/\omega_{11} > 2.0$.

•The height of the resultant seismic thrust above the base of the wall varies from 0.5*H* for the linear modulus profile to 0.64*H* for the uniform modulus profile (Fig. 18).

Effect of Poisson's ratio and damping ratio of soil backfill on seismic thrust

The results presented above were obtained using a Pois-

Fig. 11. Peak seismic thrusts for soil profiles with linear variation in *G*.

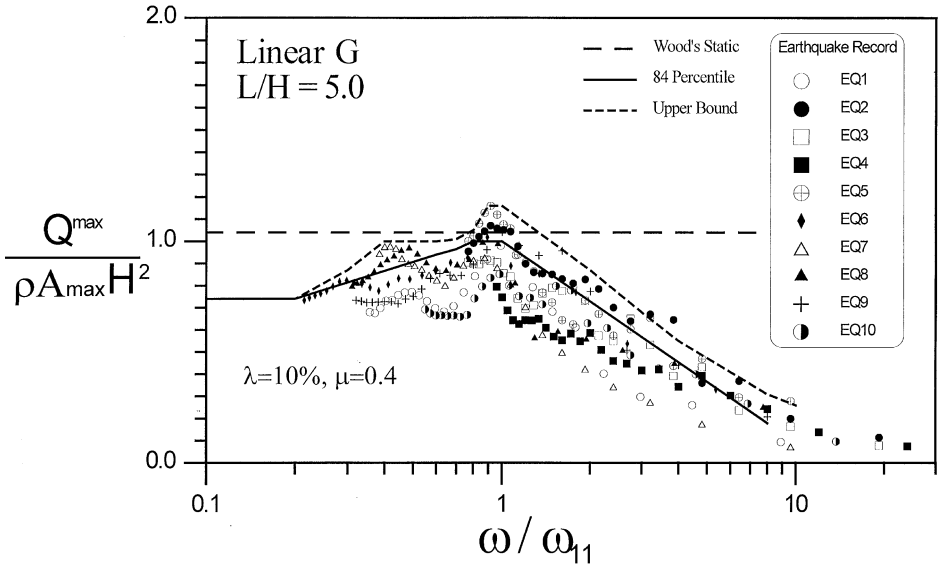

Fig. 12. Peak seismic thrusts for soil profiles with uniform *G*.

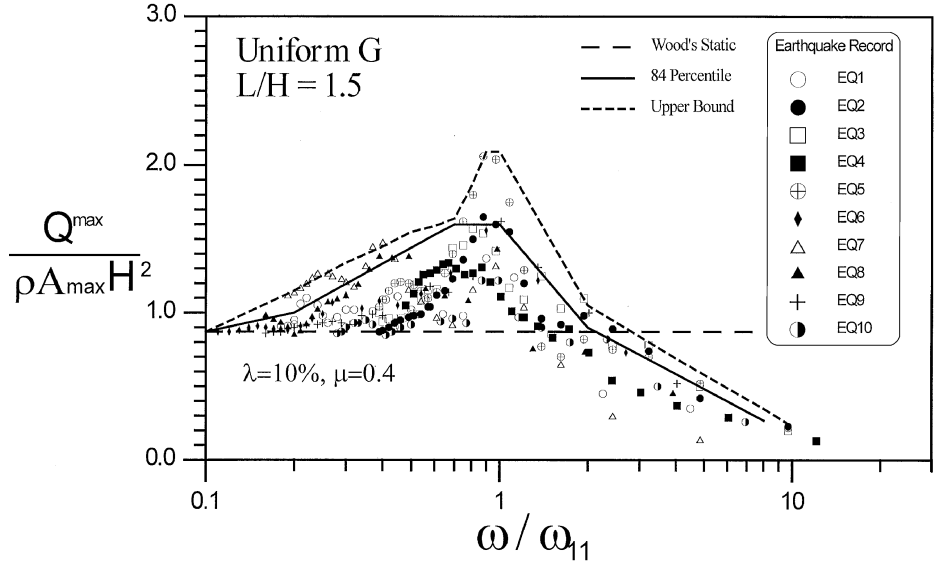

son's ratio of $\mu = 0.4$ and a damping ratio of $\lambda = 10\%$. To study the effect of Poisson's ratio μ on seismic pressures, analyses were conducted using $\mu = 0.3$ and 0.5 at an unchanged $\lambda = 10\%$. The effect of damping ratio λ on seismic pressures was studied using $\lambda = 5\%$ and 20% at an unchanged $\mu = 0.4$. These analyses were conducted using the parabolic modulus profile with $L/H = 5.0$.

Analyses were conducted for 250 combinations of ground accelerations and distributions of shear moduli for each value of μ or λ. The 84th percentile curves for peak seismic thrust ratios are shown for each μ and λ.

The effect of μ on the 84th percentile seismic pressures is shown in Fig. 19. In general, the seismic thrust ratios increase with increasing μ. The seismic thrust ratio corresponding to critical frequency ratios increases to 1.3 for $\mu = 0.5$ from 1.15 for $\mu = 0.4$ and decreases to 1.1 for $\mu = 0.3$. The correction for μ between 0.3 and 0.5 on seismic pressures can be estimated by interpolation using the curves in Fig. 19.

The effect of λ on the 84th percentile peak seismic pressures is shown in Fig. 20. In general, the peak seismic thrust ratios increase with decreasing λ. The seismic thrust ratios corresponding to critical frequency ratios increased to 1.35 at $\lambda = 5\%$ from 1.15 at $\lambda = 10\%$. The damping ratio λ has no effect on seismic thrust ratios at low frequency ratios ($\omega/\omega_{11} \leq 0.1$). The correction for λ between 5 and 20% on peak seismic pressures can be estimated by interpolating between the curves in Fig. 20.

Application of the method to nonlinear problems

The application of the proposed method to nonlinear problems is illustrated by an example. The wall–soil system has a height $H = 10$ m with $L/H = 5.0$ and a soil profile with a parabolic distribution of shear modulus with depth. The

Fig. 13. Peak seismic thrusts for soil profiles with parabolic variation in *G*.

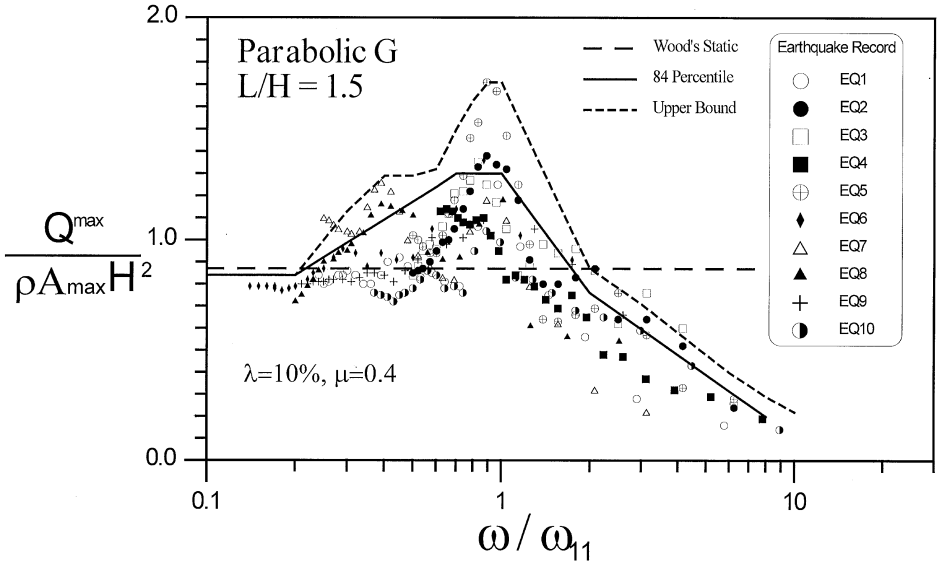

Fig. 14. Peak seismic thrusts for soil profiles with linear variation in *G*.

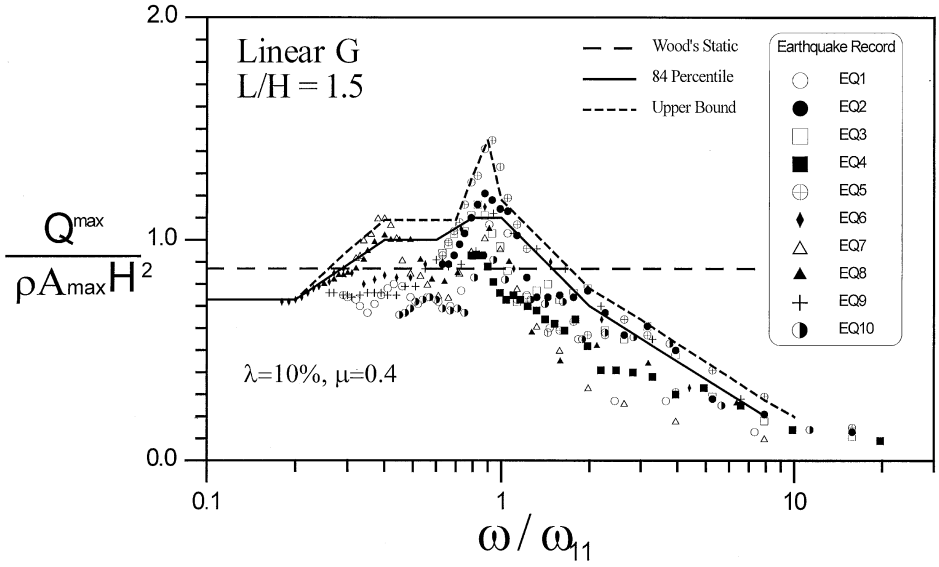

shear modulus at the base of the soil profile is assumed to be G_{soil} = 132 000 kPa corresponding to a shear wave velocity V_s = 257.0 m/s. Mass density and Poisson's ratio are ρ = 2.0 and μ = 0.4, respectively. The input motion is the El Centro acceleration record, EQ1, as described in Table 2, with a peak acceleration of A_{max} = 3.43 m/s^2.

The analysis is first conducted using the design curves presented earlier and the approximate method for estimating the fundamental frequency of the soil–wall system. Since the response is elastic, the shear moduli of the soil profile are independent of the level of input acceleration. Hence the weighted average of shear modulus in the soil profile is G^* = $0.67G_{soil}$ = 88 000 kPa. The fundamental frequency of the system is estimated using eq. [A3] in the Appendix to be ω_{11} = 37.86 rad/s. The ratio of the predominant frequency of the input motion to the fundamental frequency of the wall system is ω/ω_{11} = 0.31. The peak seismic thrust against the wall is estimated to be $Q^{max} = 0.93\,\rho H^2 A_{max}$ = 638 kN/m using the curve for parabolic *G* with *L* / *H* = 5.0 in Fig. 15.

The seismic shear strain generated by strong shaking of the backfill has two important effects due to the strain dependence of moduli and damping. It reduces the effective shear moduli in the backfill which leads to a change in the fundamental period of the soil–wall system and, hence, of the frequency ratio ω/ω_{11}. It also increases the effective damping ratios which tends to reduce the seismic response. The distribution of effective moduli and damping ratios in the freefield in the backfill may be determined using equivalent linear analysis SHAKE (Schnabel et al. 1972). These moduli and damping ratios are assumed to be reasonably representative of conditions near the wall.

The data on shear strain dependent shear moduli and damping ratios presented by Seed and Idriss (1970) were adopted. At shear strain levels of 0.0001, 0.0005, 0.001, 0.005, 0.01, 0.05, 0.1, 0.5, and 1.0%, the values of G/G_{max} were selected to be 100, 98.3, 95.8, 84.3, 74.3, 43.0, 29.6,

Fig. 15. The 84th percentile curves of peak seismic thrusts for $L / H = 5.0$.

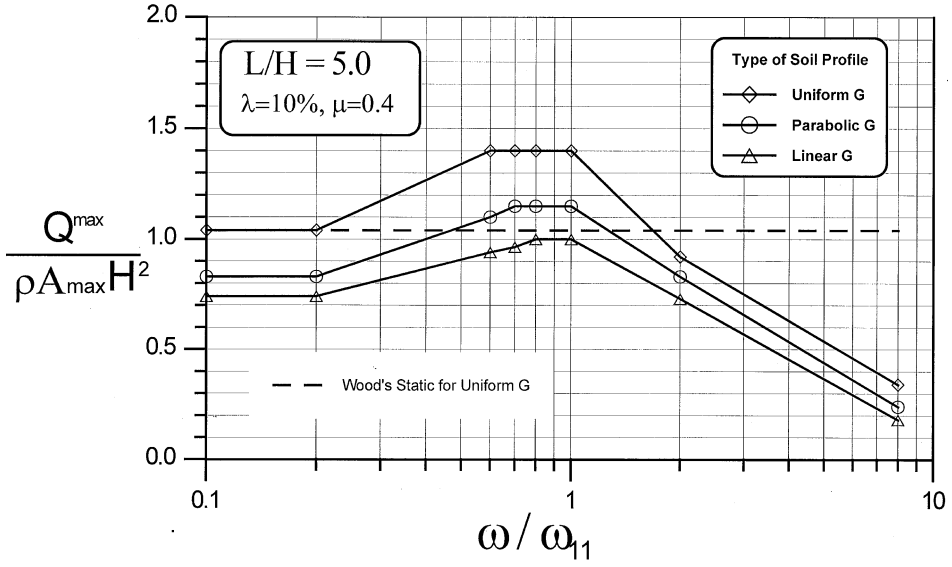

Fig. 16. The 84th percentile curves of peak seismic thrusts for $L / H = 3.0$.

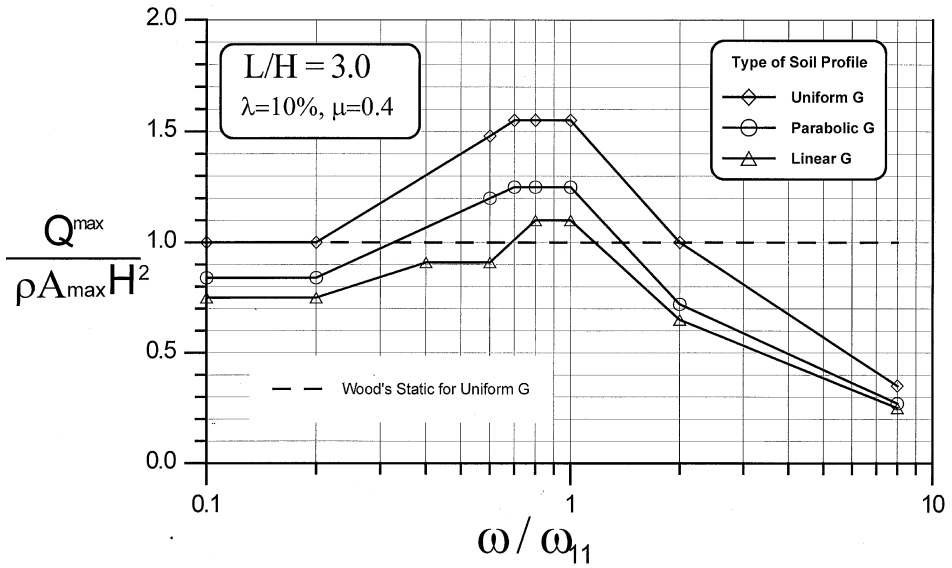

10.9, and 6.1%, respectively. The corresponding values of the damping ratio D/D_{max} are given by 0.018, 0.055, 0.073, 0.158, 0.073, 0.158, 0.275, 0.457, 0.579, 0.891, and 1.0, respectively (where D and D_{max} are the current and maximum values of the damping in percent of critical damping).

In the SHAKE analysis a soil column of the backfill was divided into 10 layers, each with a thickness of 1.0 m. The distributions of shear moduli with depth compatible with the level of shaking showed a rather uniform distribution of reduced shear moduli with depth. The values of the reduced shear moduli from the top layer to the bottom layer are 30 096, 29 807, 29 952, 30 048, 29 471, 29 615, 30 481, 31 154, 31 971, and 32 692 kPa. The weighted average of shear modulus G^* = 30 529 kPa. The average damping ratio of the soil column was $\lambda = 16.2\%$.

Equation [A1] in the Appendix is used for computing the fundamental frequency of the wall–soil system having rather uniform distribution of shear moduli with depth. The estimated fundamental frequency is ω_{11} = 20.65 rad/s, and the frequency ratio is $\omega/\omega_{11} = 0.56$. The 84th percentile seismic thrust against the wall is estimated at $\lambda = 10\%$ to be $Q^{max} = 1.36\,\rho H^2 A_{max}$ using the curve for uniform G with $L / H = 5.0$ in Fig. 15. The peak seismic thrust ratio is modified to $Q^{max} = 1.25\,\rho H^2 A_{max}$ = 858 kN/m after considering the effect of $\lambda = 16.2\%$ on seismic thrust using Fig. 20.

In this example, seismic thrust obtained from an equivalent linear analysis is 34% higher than that obtained from a linear elastic analysis. The effect of soil nonlinearity may not always increase the magnitude of seismic thrust. It depends on the combination of initial soil conditions and the level and frequency of the input motion. However, this result certainly illustrates the importance of soil nonlinearity in the evaluation of seismic thrust and the potential danger in ignoring it.

Fig. 17. The 84th percentile curves of peak seismic thrusts for $L / H = 1.5$.

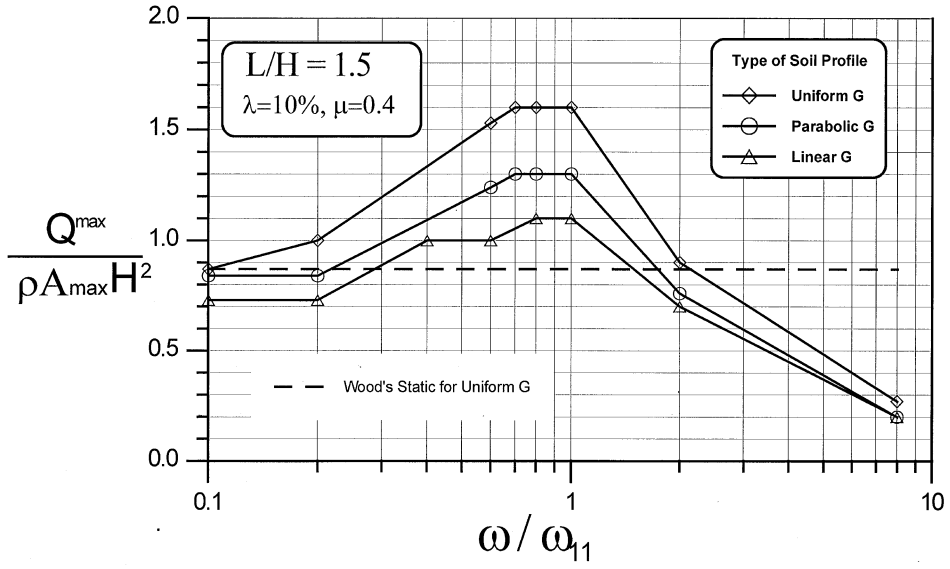

Fig. 18. Heights of application of seismic thrusts (h) for different soil profiles.

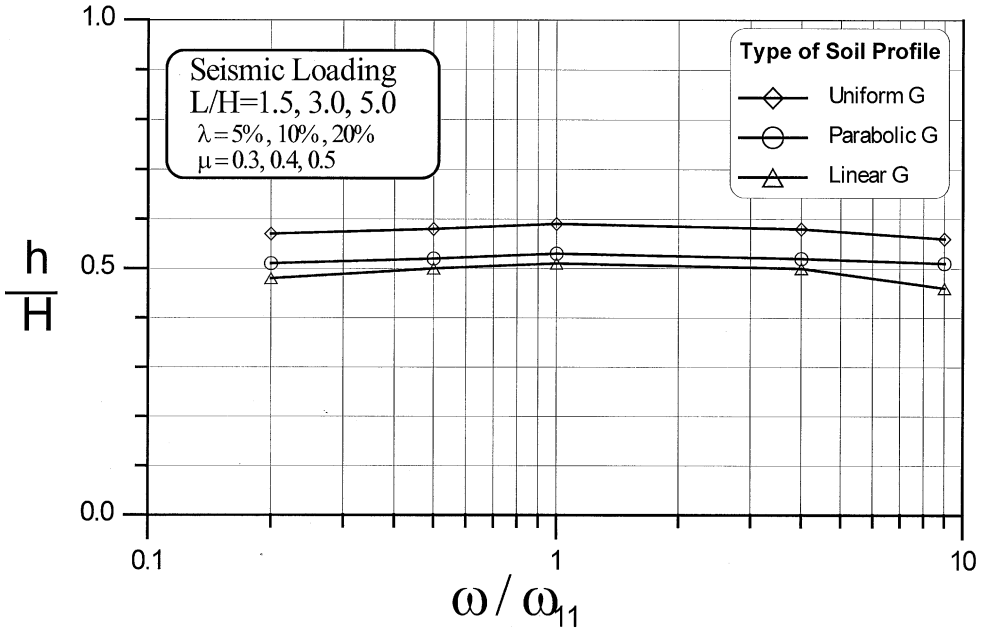

The distribution of shear modulus with depth from an equivalent linear analysis may not always be fairly uniform as in the example. For an irregular distribution of shear modulus with depth, judgement may be required in deciding the most appropriate equivalent modulus profile for use with the design curves.

Conclusions and discussion

An approximate method based on a modified shear beam model (Wu 1994; Finn et al. 1994; Wu and Finn 1996) has been used to develop charts of seismic thrusts against rigid walls for design. Peak dynamic thrusts were determined for three different soil profiles subjected to earthquake shaking. For each profile, 250 combinations of ground accelerations and distributions of soil shear moduli with depth were analysed to provide data points of peak seismic thrust ratios for the construction of design envelopes. The following are the principal results of the study.

•Design charts are presented which give upper bound and 84th percentile levels of seismic thrusts against rigid walls. These charts are based on elastic analyses with 10 different earthquake motions and 25 different moduli values for each of three different distributions of modulus with depth, namely uniform, parabolic, and linear.

•Elastic analyses for seismic thrusts were conducted with modal damping ratio $\lambda = 10\%$ and Poisson's ratio $\mu = 0.4$. Curves were developed for $\lambda = 20\%$ and 5% to allow correction for damping ratios between 5 and 20% by interpolation. Curves were developed for $\mu = 0.3$ and 0.5 to allow correc-

Fig. 19. Effect of Poisson's ratio on the 84th percentile curves of peak seismic thrust ratios.

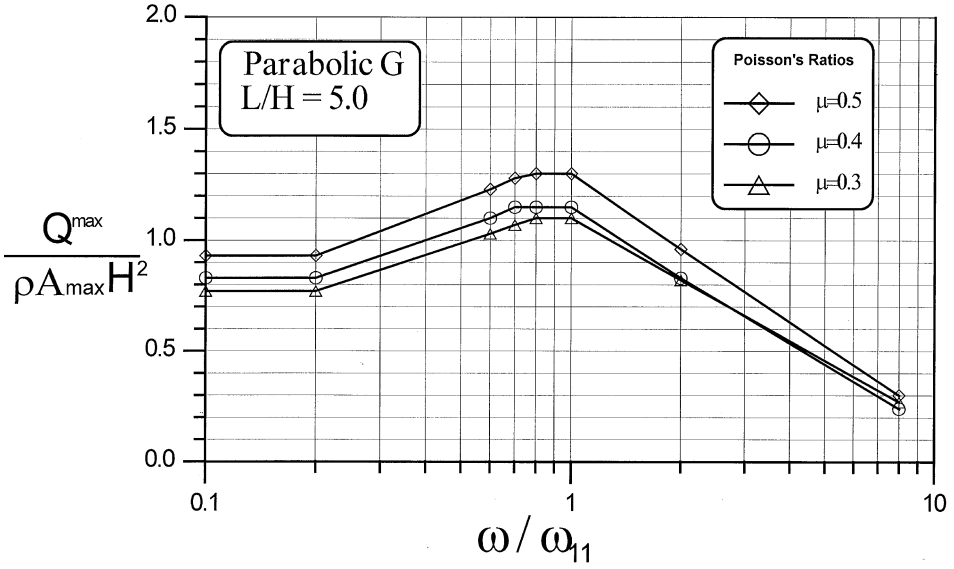

Fig. 20. Effect of damping ratio on the 84th percentile curves of peak seismic thrust ratios.

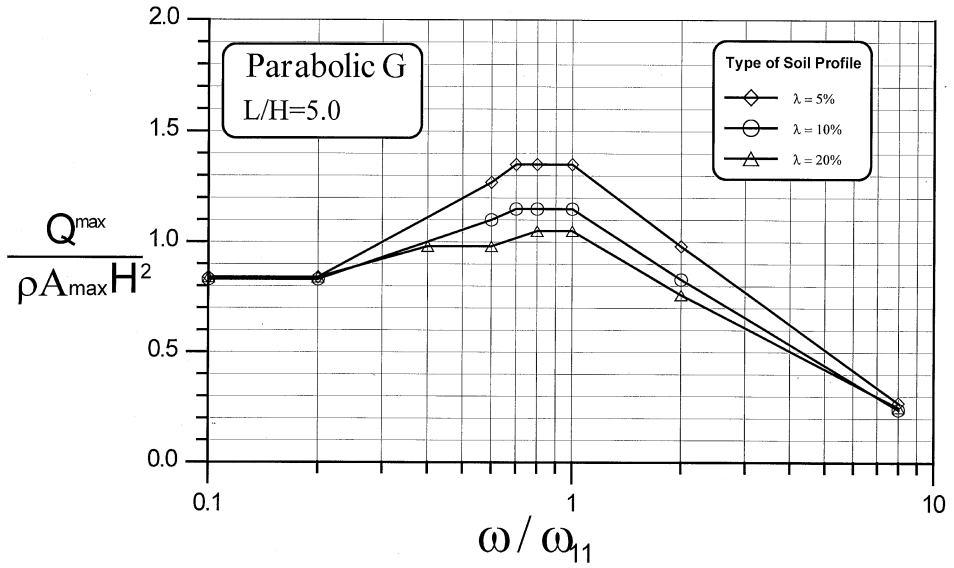

tion for Poisson's ratio between 0.3 and 0.5 by interpolation.

•The design seismic thrusts are given as functions of the fundamental frequency of the soil–wall system. An approximate method is given for estimating the frequency.

•Nonlinear behaviour results in reduced modulus and increased damping. The reduction in modulus affects the fundamental frequency of the wall–soil system. The effective reduced modulus and effective increased damping ratio may be estimated by a SHAKE analysis of the backfill. In this way, the effect of nonlinearity may be taken into account.

•Nonlinear response can result in increased seismic thrust against rigid walls.

•The static solution of Wood (1973), often used in practice, has a more limited range of applicability than previously considered for seismic excitation. It appears to be valid for $\omega/\omega_{11} < 0.2$. It underestimates seismic thrusts as the fundamental period of the wall–soil system approaches the predominant period of the earthquake motions and overestimates the seismic thrust for $\omega/\omega_{11} > 2.0$.

•The height of the resultant seismic thrust above the base of the wall varies from 0.5*H* for the linear *G* profile to 0.64*H* for the uniform *G* profile (Fig. 18).

The design envelopes were obtained under linear elastic conditions with 10% model damping. They can be extended for use under conditions of nonlinear response under strong shaking. This requires estimating the reduced shear moduli and increased damping ratios compatible with the seismic shear strains using a SHAKE analysis (Schnabel et al. 1972). The seismic design curves may then be used to estimate the seismic thrust ratio by using the fundamental frequency of the wall–soil system ω_{11} corresponding to the reduced shear moduli and correcting for the actual level of strain-compatible damping.

Acknowledgements

The financial support of the Natural Sciences and Engineering Research Council of Canada under Grant No. 1498

is gratefully acknowledged. The authors thank the reviewers for their constructive comments, which significantly improved the range of applicability of the results.

References

Arias, A., Sanchez-Sesma, F.J., and Ovando-Shelley, E. 1981. A simplified elastic model for seismic analysis of earth-retaining structures with limited displacements. *In* Proceedings of the International Conference on Recent Advances in Geotechnical Earthquake Engineering and Soil Dynamics, St. Louis, Mo., Vol. 1, pp. 235–240.

Finn, W.D.L., Wu, G., and Ledbetter, R.H. 1994. Problems in seismic soil–structure interaction. *In* Proceedings of the 8th International Conference on Computer Methods and Advances in Geomechanics, Morgantown, W.Va., pp. 139–152.

Matsuo, H., and Ohara, S. 1960. Lateral earthquake pressure and stability of quay walls during earthquakes. *In* Proceedings of the 2nd World Conference on Earthquake Engineering, Tokyo, Japan, Vol. 1, pp. 165–181.

Mononobe, N., and Matsuo, H. 1929. On the determination of earth pressure during earthquakes. *In* Proceedings of the World Engineering Conference, Vol. 9.

Okabe, S. 1926. General theory of earth pressure. Journal of the Japanese Society of Civil Engineers, **12**(1).

Scott, R.F. 1973. Earthquake-induced earth pressures on retaining walls. *In* Proceedings of the 5th World Conference on Earthquake Engineering, Rome, Italy, pp. 1611–1619.

Schnabel, P.B., Lysmer, J., and Seed, H.B. 1972. SHAKE: a computer program for earthquake response analysis of horizontally layered sites. Report No. EERC 72-12, Earthquake Engineering Research Centre, University of California, Berkeley, Calif.

Seed, H.B., and Idriss, I.M. 1970. Soil moduli and damping factors for dynamic response analyses. Report No. EERC 70-10, Earthquake Engineering Research Center, University of California, Berkeley, Calif.

Seed, H.B., and Whitman, R.V. 1970. Design of earth retaining structures for dynamic loads. *In* Proceedings of the ASCE Special Conference on Lateral Stresses, Ground Displacement and Earth Retaining Structure, Ithaca, N.Y., pp. 103–147.

Veletsos, A.S., and Younan, A.H. 1994. Dynamic soil pressures on rigid vertical walls. International Journal of Earthquake Engineering and Structural Dynamics, **23**: 275–301.

Veletsos, A.S., Parikh, V.H., and Younan, A.H. 1995. Dynamic response of a pair of walls retaining a viscoelastic solid. International Journal of Earthquake Engineering and Structural Dynamics, **24**: 1567–1589.

Wood, J.H. 1973. Earthquake-induced soil pressures on structures. Ph.D. thesis, the California Institute of Technology, Pasadena, Calif.

Wu, G. 1994. Dynamic soil–structure interaction: pile foundations and retaining structures. Ph.D. thesis, Department of Civil Engineering, the University of British Columbia, Vancouver, B.C.

Wu, G., and Finn, W.D.L. 1996. Seismic pressures against rigid walls. *In* Analysis and Design of Retaining Structures Against Earthquakes, Proceedings of the American Society of Civil Engineers Convention, Washington, D.C., pp. 1–18.

Appendix: Evaluation of the fundamental frequency ω_{11}

The fundamental frequencies of the wall–soil systems with uniform backfills can be determined from eq. [6], which is repeated as

$$[A1] \quad \omega_{11} = \frac{\pi}{2H}\sqrt{\frac{G}{\rho}}\sqrt{1+\frac{2}{1-\mu}\frac{H^2}{L^2}}$$

The reduction of soil stiffness results in a decrease of the fundamental frequency ω_{11} of the wall–soil system as shown in Fig. 15. Very good approximations to the fundamental frequencies for nonhomogeneous backfills can be obtained using eq. [A1] if G is replaced by an effective modulus G^*, which is the weighted average shear modulus over the whole depth and is given by

$$[A2] \quad G^* = \frac{\sum G_i h_i}{H}$$

Fig. A1. Variations of the fundamental angular frequencies ω_{11} of the wall–soil systems with soil stiffness (wall height H = 10.0 m; soil density ρ = 2.0). The solid lines represent eq. [A3].

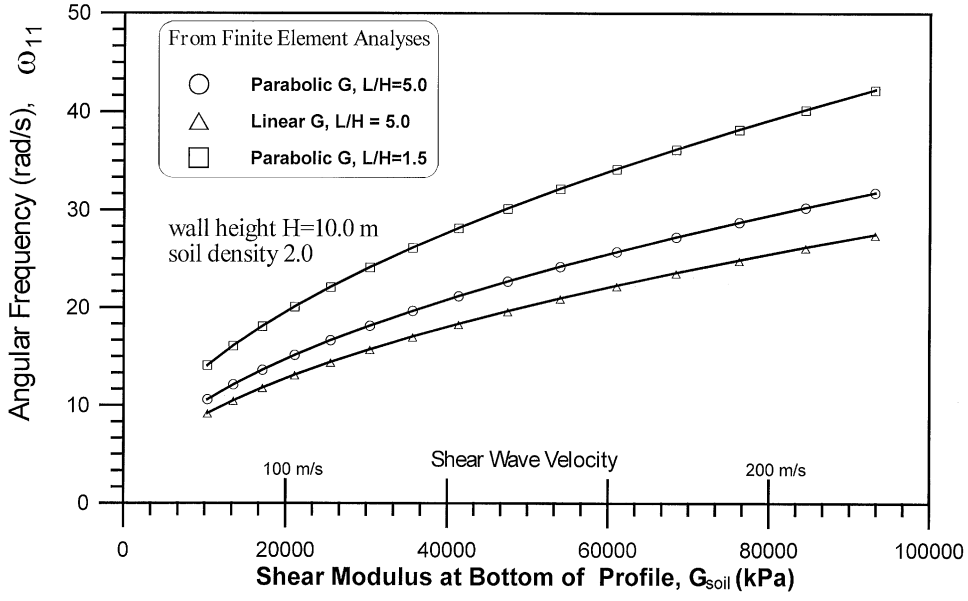

where G_i is shear modulus in the ith layer of thickness h_i. For a parabolic soil profile with G_{soil} at a depth H, $G^* = 0.67G_{soil}$ is obtained; for a linear soil profile, $G^* = 0.5G_{soil}$ is obtained.

The accuracy is improved by the introduction of a correction factor R_f, which ranges from 0.97 to 1.08 as L/H ranges from 1.5 to 5.0. In practice this correction is not necessary.

For nonhomogeneous soil profiles, the fundamental frequencies ω_{11} of wall–soil systems may be estimated for practical purposes from eq. [A1] with G replaced by G^* and a correction factor R_f.

$$[A3] \quad \omega_{11} = R_f \frac{\pi}{2H}\sqrt{\frac{G^*}{\rho}}\sqrt{1+\frac{2}{1-\mu}\frac{H^2}{L^2}}$$

where $R_f = 0.97$ for $L/H = 1.5$ and 1.08 for $L/H = 5.0$.

The fundamental frequencies ω_{11} computed from eq. [A3] are also shown by the solid lines in Fig. A1, which indicates that the proposed equation works very well for all cases investigated.